Bulk sensing experiments using a surface-plasmon interferometer

Peter Debackere,* Roel Baets, and Peter Bienstman

Photonics Research Group, Department of Information Technology–Ghent University–IMEC, Sint-Pietersnieuwstraat 41, 9000 Gent, Belgium
**Corresponding author: Peter.Debackere@intec.UGent.be*

Received May 12, 2009; revised August 6, 2009; accepted August 10, 2009; posted August 21, 2009 (Doc. ID 111334); published September 14, 2009

Experimental evidence supporting the use of a surface-plasmon interferometer as a biosensor is presented. The device is shown to be capable of bulk refractive index sensing (bulk refractometry) and has a spectral interrogation sensitivity of 315.145 nm/refractive index unit. © 2009 Optical Society of America

OCIS codes: 130.3120, 130.6010, 240.6680.

Evanescent field sensors provide a promising means for the label-free detection of target molecules and for the real-time monitoring of solutions and binding events that occur near the sensor surface. Waveguide sensors constructed in semiconductor material such as silicon-on-insulator (SOI) can have an extremely small footprint, be integrated into compact arrays, and be readily combined with fluidic components, promising features for potential lab-on-a-chip applications [1]. Furthermore, monolithic integration of sensors with electronics is also feasible. The nanophotonic SOI platform is compatible with well-established complementary metal-oxide semiconductor (CMOS) fabrication and characterization technologies, providing a potential route to low-cost, high-volume manufacturing. Of the different approaches toward integrated SOI label-free affinity sensors, microring resonators are perhaps the most promising candidates [2,3].

However, in the field of direct real-time affinity sensing, surface-plasmon-resonance (SPR) biosensors are a well-established technology [4,5]. Owing to the very strong evanescent fields near the interface, surface plasmons promise to be very sensitive to refractive index changes. Moreover, Au boasts the advantage that it is a biocompatible material and that a very mature thiol chemistry can be used for the functionalization of this layer. Drawbacks are that state-of-the-art SPR devices are bulky and expensive and that the integration with micofluidics and the route toward multiparameter analysis are difficult.

A surface-plasmon interferometer combines the best of both worlds [3,6]. The principle is based on the interference of two decoupled surface-plasmon modes propagating on either side of a thin metallic layer embedded into a silicon waveguide. The theoretical concept and feasibility were previously reported in [6]. Theoretical results predict that this device would be capable of detecting very small refractive index changes (10^{-6} RIUs, refractive index units) for a device that has a physical footprint of only 100 μm^2. In this Letter we present the first experimental evidence of such a device, to our knowledge.

The surface-plasmon interferometer is schematically depicted in Fig. 1. Upon reaching the gold-clad layer, a dielectric TM-polarized mode guided by the silicon membrane slab waveguide excites two surface-plasmon modes, one at the upper and one at the lower interface of the gold layer. Owing to the highly asymmetric cladding layers, these modes are not coupled; therefore their phase velocities are entirely determined by the refractive index of the upper and lower dielectric. At the end of this section, interference of the two surface-plasmon modes results in a dielectric mode launched in the output waveguide. This explains the sensing functionality of the interferometer; a change in the refractive index of the medium above the gold layer results in a phase difference between the two surface-plasmon modes and, consequently, in a change of output intensity.

Proof-of-principle samples consisted of a silicon substrate, 2 μm of high-density plasma silicon dioxide, and 220 nm of amorphous silicon (a-Si), deposited using a plasma-enhanced chemical vapor deposition process with SiH_4 and He gases [7]; fabrication was done using deep-UV lithography. The length of the sensing area was 8 μm; waveguides were 3 μm wide. The etch depth of the sensor region in the Si was 70 nm; the Au layer was deposited using vacuum evaporation and was 37 nm thick. A focused ion-beam cross section of the fabricated device can be seen on the right side of Fig. 2.

Light from a single-mode fiber was coupled into the sample using a lensed fiber; outcoupling occurs

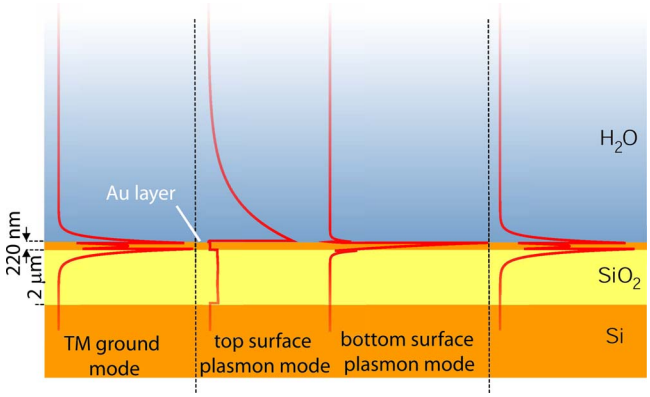

Fig. 1. (Color online) Schematical setup of the proposed structure, $|E_x|$ field shown (perpendicular to the interface).

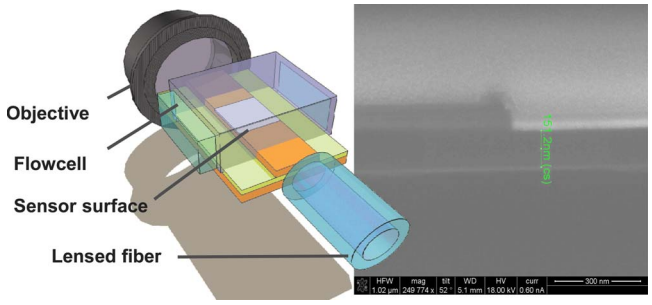

Fig. 2. (Color online) Left, schematic representation of the surface-plasmon interferometer, the flowcell, and the measurement setup; right, focused ion beam cross section of the fabricated device.

through an objective. Measurements were performed using a tunable laser (output power 5 mW) and power detector; a polarizer has been used in front of the detector in order to ensure that only TM-polarized light is measured. Experiments were not temperature stabilized.

Proof of principle was obtained by flowing deionized water, an aqueous solution of 2 m. % and 10 m. % of NaCl over the sensor surface (Table 1). The spectra for these measurements are presented in Fig. 3. Standard-deviation error bars represent measurements of several spectra with an interval of 10 min to ensure that the steady-state response was measured. One can clearly see that the position of the spectral minimum is blueshifted as a function of increasing analyte refractive index, which is in good agreement with theoretical predictions.

To quantify the sensitivity of the device with respect to bulk refractive index changes, deionized water, an aqueous solution of 2 m. %, 4 m. %, 6 m. %, and 8 m. % of NaCL were flown over the sensor surface, using a flow cell to avoid evaporation. At 20 °C the refractive index of an aqueous solution of NaCl varies with 0.0017151 RIUs per mass % [8,9]. A two-point moving average filter and spectral normalization has been utilized to analyze the spectral data. Sensitivity S_{RIU} [nm/RIU] for this sensor was determined by calculating the wavelength of destructive interference using a Lorentzian curve-fitting algorithm [10]; the standard deviation error $\delta\lambda_{\mathrm{min}}$ is due partly to the dip-finding algorithm (dependence of the dip position as a function of threshold value is taken into account) and partly to measurement errors. Results are given in the table below. Using this data we can estimate the general sensitivity S_{RIU} of this device to be 435.454 nm/RIU. The wavelength of

Table 1. λ_{min}, $\delta\lambda_{\mathrm{min}}$, and Detection Limit (DL) as a Function of NaCl Concentration[a]

Solution	λ_{min}[nm]	$\delta\lambda_{\mathrm{min}}$[nm]	DL[RIU]
H_2O	1539.414	0.447	1.027×10^{-3}
2 m. %	1538.325	0.624	1.433×10^{-3}
4 m. %	1536.933	0.528	1.213×10^{-3}
6 m. %	1534.197	1.291	2.965×10^{-3}
8 m. %	1534.010	0.913	2.096×10^{-3}

[a]Sensitivity: 435.454 ± 0.485 nm/RIU.

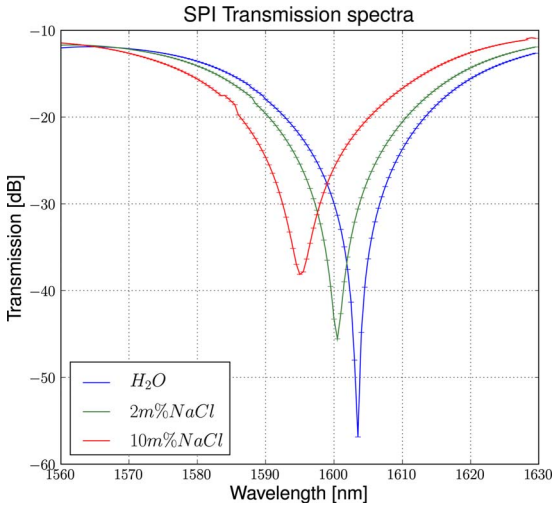

Fig. 3. (Color online) Simulated transmission spectra for H_2O, 2 m. % NaCl, and 10 m. % Nacl. Simulations done using CAMFR, an in-house developed eigenmode solver using adaptive spatial resolution [11]. Theoretical sensitivity is equal to 392 nm/RIU.

minimal transmission versus the refractive index of the analyte flown over the sensor surface is depicted in Fig. 4.

The observed positions of maximum spectral attenuation are in agreement with the theoretical model [6], as can be seen in Fig. 5. Sensitivity S_{RIU} is larger than the theoretically obtained value. The standard deviation of S_{RIU}, although an indication of the linearity of the sensor response, does not represent the accuracy of the sensitivity value, since the linear regression algorithm does not take measurement errors into account. Therefore the value of S_{RIU} was calculated in Monte Carlo simulations (10^6 iterations), using added Gaussian noise with a standard deviation equal to the calculated standard deviation of the spectral minima. The resulting value for

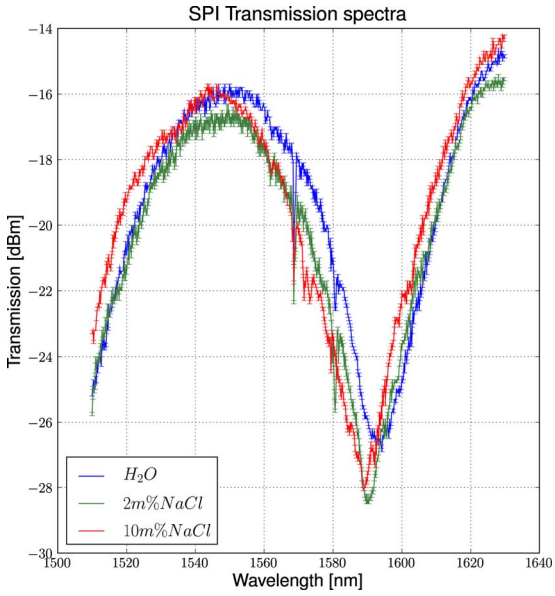

Fig. 4. (Color online) Measured transmission spectra for H_2O, 2 m. % NaCl, and 10 m. % Nacl, fiber-to-detector spectra.

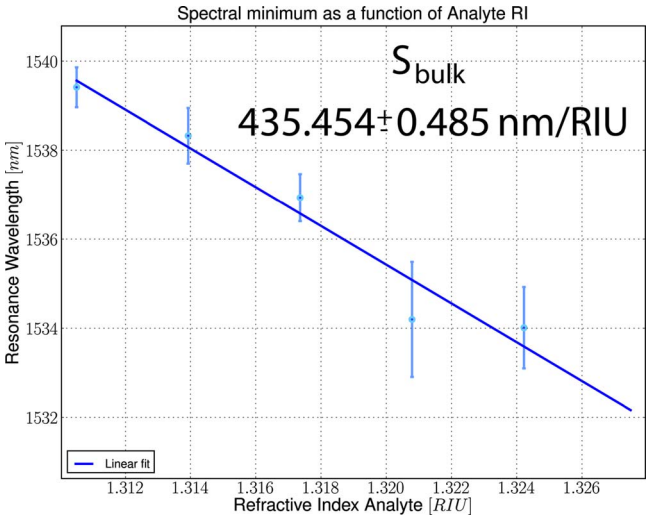

Fig. 5. (Color online) λ_{min} as a function of NaCl concentration; the solid line is a linear fit to calculated λ_{min} values.

S_{RIU} is normally distributed, the mean value is 435.541 nm/RIU, the standard deviation 72.543 nm/RIU. Theoretical sensitivity lies well within one standard deviation of this calculated value for S_{RIU}.

Departures from the theory in both position of minimal transmission and slope of the curves are probably caused mainly by the scattering of waves at imperfect boundaries of the Au layer at the beginning and end sections of the Au layer (lithographic inaccuracies) and the surface roughness of the Au layer.

The experimental determination of the maximum mode attenuation of the device is limited by polarization coupling in the waveguide itself and by performance of polarizing optics [12].

In this Letter we have presented a proof of principle for an integrated surface-plasmon interference sensor. Qualitative agreement between measurement results and theoretical data has been obtained. Furthermore, we have shown this device capable of detecting bulk refractive index changes, a first and indispensable step toward label-free biosensing. The measured blueshift, although not yet as large as theoretically predicted, shows the potential of this device to be used as a sensitive and label-free biosensor.

This work was carried out in the context of the GOA project (Ghent University) and was supported by the Belgian IAP PHOTON network. P. Debackere would like to thank S. Selvaraja for fabricating the a-Si samples.

References

1. W. Bogaerts, R. Baets, P. Dumon, V. Wiaux, S. Beckx, D. Taillaert, B. Luyssaert, J. Van Campenhout, P. Bienstman, and D. Van Thourhout, J. Lightwave Technol. **23**, 401 (2005).
2. K. De Vos, I. Bartolozzi, E. Schacht, P. Bienstman, and R. Baets, Opt. Express **15**, 7610 (2007).
3. R. Baets, D. Taillaert, W. Bogaerts, P. Dumon, K. De Vos, P. Debackere, S. Scheerlinck, and D. Van Thourhout, in *Conference on Lasers and Electro-Optics* (Optical Society of America, 2007), pp. 1221–1222.
4. X. D. Hoa, A. G. Kirk, and M. Tabrizian, Biosens. Bioelectron. **23**, 151 (2007).
5. J. Homola, Anal. Bioanal. Chem. **377**, 528 (2003).
6. P. Debackere, S. Scheerlinck, P. Bienstman, and R. Baets, Opt. Express **14**, 7063 (2006).
7. S. Selvaraja, E. Sleeckx, M. Schaekers, W. Bogaerts, D. Van Thourhout, P. Dumon, and R. Baets, Opt. Commun. **182**, 1767 (2009).
8. D. R. Lide, *CRC Handbook of Chemistry and Physics* (CRC Press, 2004).
9. S. Hiu and X. G. Huang, Sens. Actuators B **126**, 579 (2007).
10. C. Thirstrup and W. Zong, Sens. Actuators B **106**, 796 (2005).
11. P. Debackere, P. Bienstman, and R. Baets, Opt. Quantum Electron. **38**, 857 (2006).
12. J. Homola, J. Čtyrocký, M. Skalský, J. Hradilová, and P. Kolářová, Sens. Actuators B **38–39**, 286 (1997).